PHOTONICS Research

Reflection sensitivity of dual-state quantum dot lasers

Zhiyong Jin,[1,†] Heming Huang,[2,†] Yueguang Zhou,[3] Shiyuan Zhao,[2] Shihao Ding,[2] Cheng Wang,[4] Yong Yao,[1] Xiaochuan Xu,[1] Frédéric Grillot,[2,5] and Jianan Duan[1,*]

[1]State Key Laboratory on Tunable Laser Technology, School of Electronic and Information Engineering, Harbin Institute of Technology, Shenzhen 518055, China
[2]LTCI, Telecom Paris, Institut Polytechnique de Paris, 91120 Palaiseau, France
[3]DTU Electro, Department of Electrical and Photonics Engineering, Technical University of Denmark, 2800 Lyngby, Denmark
[4]School of Information Science and Technology, ShanghaiTech University, Shanghai 201210, China
[5]Center for High Technology Materials, The University of New-Mexico, Albuquerque, New Mexico 87106, USA
[†]These authors contributed equally to this paper.
*Corresponding author: duanjianan@hit.edu.cn

Received 28 April 2023; revised 24 July 2023; accepted 7 August 2023; posted 8 August 2023 (Doc. ID 494393); published 27 September 2023

This work experimentally and theoretically demonstrates the effect of excited state lasing on the reflection sensitivity of dual-state quantum dot lasers, showing that the laser exhibits higher sensitivity to external optical feedback when reaching the excited state lasing threshold. This sensitivity can be degraded by increasing the excited-to-ground-state energy separation, which results in a high excited-to-ground-state threshold ratio. In addition, the occurrence of excited state lasing decreases the damping factor and increases the linewidth enhancement factor, which leads to a low critical feedback level. These findings illuminate a path to fabricate reflection-insensitive quantum dot lasers for isolator-free photonic integrated circuits.

https://doi.org/10.1364/PRJ.494393

1. INTRODUCTION

Continued growth in demand for sensing, communication, and computing has given rise to photonic integrated circuits (PICs) for applications such as LiDAR for self-driving systems, next-generation artificial intelligence systems, data transmission in 5G/6G optical networks, and quantum communications [1–3]. Particularly, silicon-based PICs with dense integration of lasers, modulators, and passive components are evolving rapidly from proof-of-concept demonstrations to commercialized products due to their advantages in terms of size, weight, cost, and power consumption. One of the biggest challenges for PICs is optical feedback that comes from either unwanted parasitic reflections or leakage from other adjacent components. This feedback degrades the coherence of on-chip lasers and enhances relative intensity noise (RIN), leading to strong laser instability such as a chaotic state or coherent collapse [4,5]. To overcome this issue, optical isolators must be appended to on-chip lasers for practical applications. However, the integration of optical isolators on the silicon substrate is quite challenging due to their bulky size and incompatibility with CMOS fabrication techniques [6]. In this context, on-chip lasers with intrinsic insensitivity to optical feedback are desirable in isolator-free PICs for optical sensing, communication, and computing systems.

Quantum dot (QD) lasers are considered the most promising on-chip light sources because QD gain material is available for both hybrid and monolithic integration on silicon, due to its high tolerance to threading dislocation defects [7–11]. Furthermore, compared with their quantum well (QW) counterparts, the intrinsic tight three-dimensional carrier confinement in QDs leads to numerous outstanding laser characteristics such as low threshold current density [12–16], high temperature stability [17–20], and low optical noise [21,22]. For QW lasers, laser emission always comes from the ground state (GS) transition, which is not the case for QD lasers. By continuously increasing pump currents, QD lasers exhibit a propensity to operate in the dual state at elevated output power, wherein the coexistence of GS and excited state (ES) emissions is obtained. This unique peculiarity in QD lasers is attributed to the unclamped gain and cascade-like carrier relaxation process [23–25]. Compared with sole GS QD lasers, QD lasers operating on sole ES exhibit not only relatively wide modulation bandwidth [26] due to higher differential gain [27] and faster carrier relaxation rate [28], but also more complex routes to chaos due to a lower relaxation oscillation frequency (ROF) [29–31], which is of great interest for random number generation [32]. Furthermore, dual-state lasing QD lasers exhibit lower intensity noise and larger modulation bandwidth than that of sole GS or ES QD lasers, which is due to the

quasi-antiphase dynamics in the carrier relaxation process [33–35]. Dual-state lasing dynamics has been theoretically proved to be governed by the effect of a phonon bottleneck and inhomogeneous broadening [36]. The dual-state emission character of QD lasers opens up the possibility of many external perturbation scenarios that are of interest for both physics and engineering; foremost among them is bistability with a switching mechanism [37]. For instance, a transition from full GS emission to full ES emission in QD lasers can be realized through optical injection [38,39]. The nature of this intrinsic bistability and Q-switching dynamics in QD lasers contributes to the development of optical storage elements [40–42], optical triggers [43–45], as well as all-optical gates [39].

For optical feedback, QD lasers emitting on the sole GS have been shown to be highly resistant to both long-delay and short-delay external feedback due to their low linewidth enhancement factor (α_H-factor) and high damping factor [46]. These lasers also exhibit error-free transmission under optical feedback in both external modulation and direct modulation configurations [47–49]. In contrast, QD lasers emitting on sole ES are more sensitive to optical feedback, which is attributed to the smaller damping rate and stronger partition noise [29–31]. When QD lasers operate in the dual state, the introduction of optical feedback leads to bistable operation where a power drop in the GS and an intensity burst in the ES are obtained [50–52].

This paper presents an experimental and theoretical investigation on the reflection sensitivity of dual-state QD lasers when subjected to external optical feedback. Experiment results show that the critical feedback level of dual-state QD lasers strongly depends on the occurrence of ES, demonstrating that reflection tolerance is greatly degraded at the ES lasing threshold. To interpret the underlying mechanism of this phenomenon, we establish a three-level rate equations model of a dual-state QD laser, by taking into account the effect of optical feedback. To assess the feedback resistance of dual-state QD lasers, the critical feedback level is determined by analyzing the simulated bifurcation diagram. Theoretical results align well with experimental observations, demonstrating that the damping factor and ROF significantly decrease while the α_H-factor substantially increases at the ES lasing threshold, which finally affects the laser resistance to external optical feedback. Furthermore, higher ES-GS energy separation exhibits a positive association with the ES-GS threshold ratio, which can strengthen feedback insensitivity. This paper provides an in-depth investigation into the reflection sensitivity of dual-state QD lasers, emphasizing the significance of energy-level engineering in fabricating feedback-insensitive dual-state QD lasers for PICs without on-chip isolators.

2. DEVICE AND MEASUREMENT

A. QD Laser and Experiment Setup

For the QD laser in this study, the active region consists of 10 QD layers grown by solid source molecular beam epitaxy (MBE) on n+ GaAs (100) substrates. The QDs are directly deposited on the GaAs matrix at 485°C by deposition of 2.5 monolayers (ML) InAs at the growth rate of 0.083 ML/s and then covered with a 5 nm thick $In_{0.15}Ga_{0.85}As$ layer, which results in a surface density of about 3×10^{10} to 5×10^{10} cm^{-2}. The dimensions of the QDs are typically within 15 to 20 nm in diameter and 3 to 5 nm in height, while the GaAs spacer is 33 nm in thickness. The laser is processed to have a 1 mm long cavity with as-cleaved facets and a 2 μm wide waveguide etched through the active area. The laser has low threshold current density, high differential efficiency, and high characteristic temperature [53]. At room temperature of 20°C, the threshold currents of the QD laser for GS and ES transitions (I_{th}^{GS}, I_{th}^{ES}) are 16.5 and 186 mA, respectively. The corresponding ratio between ES and GS threshold currents is 11.3. Dual-state lasing operation can be achieved by increasing the bias current of the QD laser, as depicted in Fig. 1. The red and yellow blocks in Fig. 1(a) highlight the optical gain of GS and ES transitions, respectively. Dashed lines (1) and (2) in Fig. 1(b) mark the bias currents in Figs. 1(a1) and 1(a2), respectively. The laser first exhibits GS lasing at lower bias currents while the peak wavelength is redshifted with the increase of current. The optical spectrum splits into two peaks separated by approximately 90 nm when the ES threshold current is exceeded.

The experiment setup for investigating the feedback sensitivity of QD lasers is depicted in Fig. 2. The light emitted from

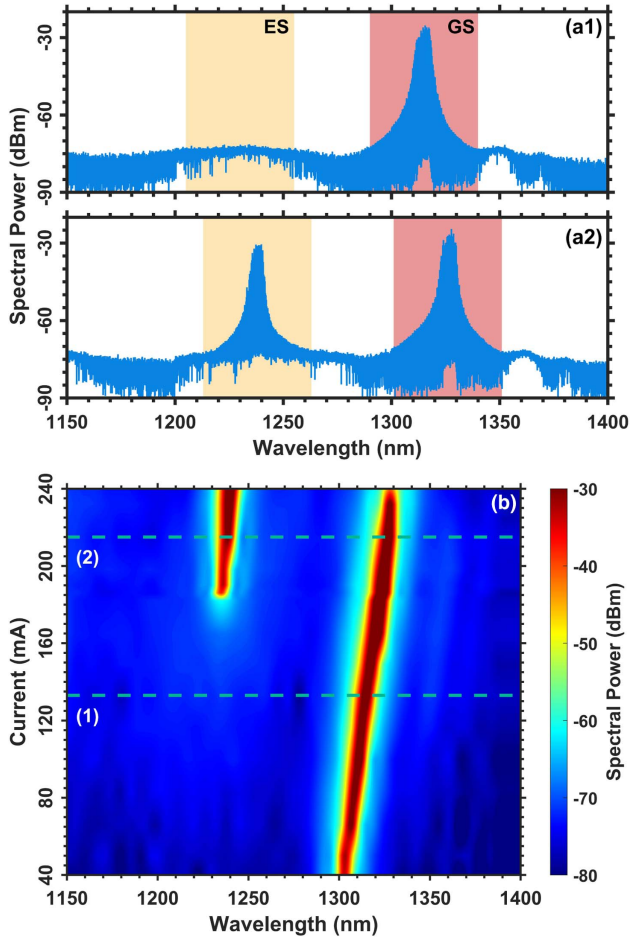

Fig. 1. Optical spectrum of (a1) sole GS lasing and (a2) dual-state lasing of QD lasers. (b) Optical spectrum mapping with the increase of bias current for the dual-state QD laser. Dashed lines (1) and (2) in (b) mark the bias currents of (a1) and (a2), respectively.

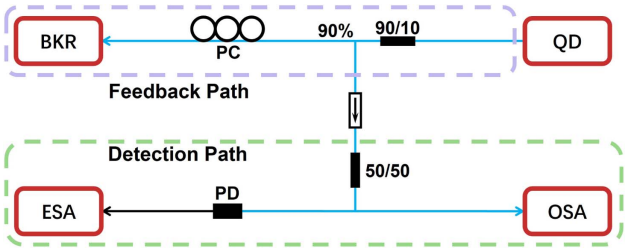

Fig. 2. Experimental setup for investigating the feedback sensitivity of QD lasers. BKR, backreflector; PC, polarization controller; OSA, optical spectrum analyzer; PD, photodiode; ESA, electrical spectrum analyzer.

the QD laser is coupled by an anti-reflection-coated lens-end fiber and split by a 90/10 coupler into two paths; 90% of the coupled power is sent to the feedback path, while the remaining 10% is for detection. A backreflector (BKR) integrated with a mirror and variable attenuator is plugged to generate reflection. The polarization controller is inserted to compensate for fiber dispersion in the feedback path. In this case, the external cavity is composed of mentioned fiber components and necessary fiber optics patch cables, leading to a cavity length of 7 m, which corresponds to a long-delay feedback configuration [54]. The feedback strength (f_{ext}) is defined as the ratio between the power returned to the laser and emitted by the laser, which can be adjusted by the BKR. The maximal f_{ext} can reach −6.1 dB in the measurement with the loss of laser-to-fiber coupling and fiber connection taken into account. An isolator can prevent additional feedback from the detection path. The feedback dynamics of a dual-state QD laser is investigated through an optical spectrum analyzer (OSA) and an electrical spectrum analyzer (ESA). Since the ROF of QD lasers is of the order of several GHz [27], the 12 GHz bandwidth of the photodiode (PD) is sufficient in the experiment.

B. Optical Feedback Measurement

Figure 3 depicts the optical and radio frequency (RF) spectrum mappings as a function of the feedback strength for different bias currents of 0.72×, 1×, and 1.25 × $I_{\text{th}}^{\text{ES}}$. The progression of the longitudinal mode of the gain peak and dynamical behavior in the RF domain is depicted in columns 1 and 2, respectively. With the increase of feedback strength, the narrow modal linewidth in optical spectra and the absence of coherence collapse in RF spectra can be maintained until the critical feedback level (r_{crit}) is exceeded. r_{crit} corresponds to the birth of laser destabilization, beyond which the laser is no longer stable against optical feedback where strong longitudinal mode broadening, the first Hopf bifurcation, and the onset of coherence collapse take place [47]. The QD laser exhibits weak resistance to optical feedback with $r_{\text{crit}} = -24.0$ dB at the ES threshold current compared to the case of 0.72 × $I_{\text{th}}^{\text{ES}}$, which has larger r_{crit} of −15.9 dB, meaning that the stability of GS lasing is degraded when approaching dual-state lasing. It is contributed by the lower damping factor and larger α_H-factor, which is theoretically confirmed in Section 3.C. Once ES lasing occurs, the feedback resistance re-increases to $r_{\text{crit}} = -14.8$ dB at 1.25 × $I_{\text{th}}^{\text{ES}}$, which results from a reduction of the α_H-factor

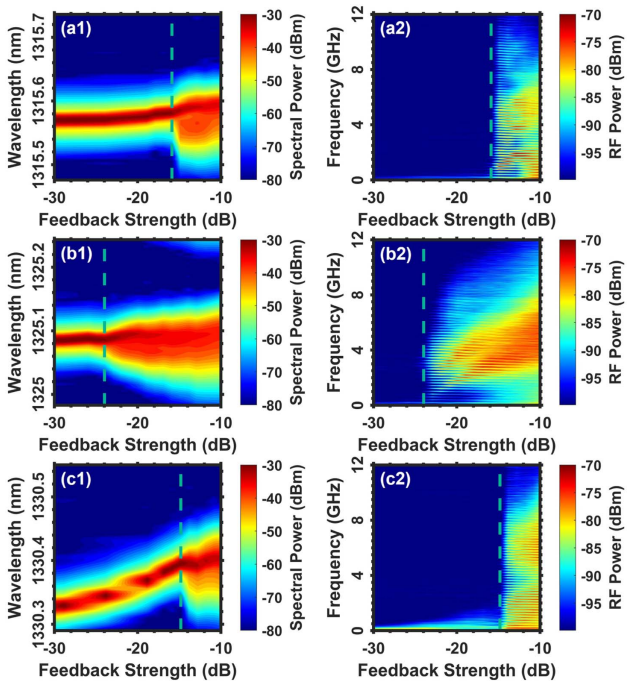

Fig. 3. Optical (column 1) and RF (column 2) spectrum mappings for QD laser operating at (a) 0.72×, (b) 1×, and (c) 1.25 × $I_{\text{th}}^{\text{ES}}$. Dashed lines mark the critical feedback levels.

associated with the ES transition induced by the larger differential gain. In addition, it is important to stress that any further increase of the pump current also raises the damping factor accordingly, resulting in restabilization of the lasers against optical feedback. The whole process of r_{crit} variation with increasing bias current is shown later in Fig. 8 to compare with simulation results. Figure 4 compares the optical and RF spectra for high f_{ext} of −9.9 dB and low f_{ext} of −29 dB at the ES lasing threshold. At a high feedback level, the laser experiences the coherence collapse state with strong broadening of the Fabry-Perot (FP) modes in both GS and ES as well as intense chaotic oscillations observed in the RF domain. In the following section, the three-level rate equations are established to further investigate the complete optical feedback dynamics in dual-state QD lasers.

3. THEORY AND SIMULATION

A. QD Laser Model

In this work, the three-level rate equations model is based on the electronic structure of the QD laser illustrated in Fig. 5. This numerical model is built on the assumption that the active region consists of one QD ensemble, which means that all QDs have the same size. Thus the inhomogeneous broadening of the gain profile can be ignored in this model. Furthermore, the electrons and holes are assumed to be neutral excitons that are injected directly into the two-dimensional carrier reservoir state (RS) from the electrodes. It is noted that the carrier dynamics in the three-dimensional separate confinement heterostructure (barrier) layers is not considered in this model. The ES is thought to be four-fold degenerate, while the GS is

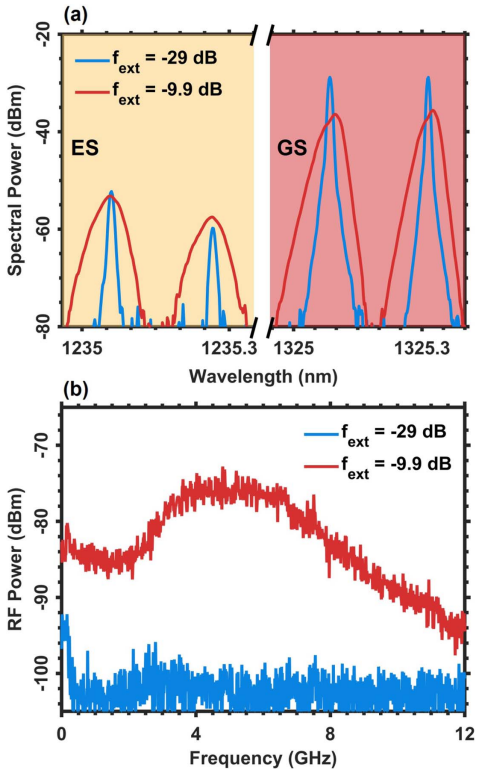

Fig. 4. (a) Optical and (b) RF spectra of QD lasers operated at $1 \times I_{\mathrm{th}}^{\mathrm{ES}}$ subject to high feedback strength of –9.9 dB (red) and low feedback strength of –29 dB (blue).

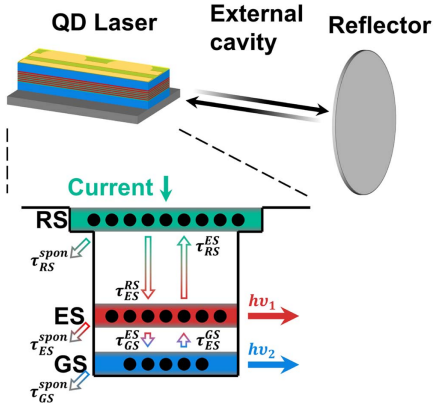

Fig. 5. Schematic representation of the electronic structure and carrier dynamics of QD lasers under optical feedback.

thought to be two-fold degenerate. Carriers are captured into the ES from RS with captured time $\tau_{\mathrm{ES}}^{\mathrm{RS}}$ and then followed by a relaxation process into the GS with relaxation time $\tau_{\mathrm{GS}}^{\mathrm{ES}}$. On the other hand, owing to the thermal excitation, carriers are excited from the GS to the ES with escape time $\tau_{\mathrm{ES}}^{\mathrm{GS}}$, and from the ES to the RS with escape time $\tau_{\mathrm{RS}}^{\mathrm{ES}}$. Carriers in the three levels (RS, ES, GS) recombine spontaneously with emission times $\tau_{\mathrm{RS,ES,GS}}^{\mathrm{spon}}$, respectively. Both the GS and ES exhibit stimulated emission simultaneously under optical feedback. Based on this model, the corpuscular rate equations including the temporal differential of the carrier numbers $N_{\mathrm{RS,ES,GS}}$, photon numbers $S_{\mathrm{ES,GS}}$, and phases of electric fields $\phi_{\mathrm{ES,GS}}$ are expressed as

$$\frac{\mathrm{d}N_{\mathrm{RS}}}{\mathrm{d}t} = \frac{I}{q} + \frac{N_{\mathrm{ES}}}{\tau_{\mathrm{RS}}^{\mathrm{ES}}} - \frac{N_{\mathrm{RS}}}{\tau_{\mathrm{ES}}^{\mathrm{RS}}}(1-\rho_{\mathrm{ES}}) - \frac{N_{\mathrm{RS}}}{\tau_{\mathrm{RS}}^{\mathrm{spon}}} + F_{\mathrm{RS}}, \tag{1}$$

$$\frac{\mathrm{d}N_{\mathrm{ES}}}{\mathrm{d}t} = \left(\frac{N_{\mathrm{RS}}}{\tau_{\mathrm{ES}}^{\mathrm{RS}}} + \frac{N_{\mathrm{GS}}}{\tau_{\mathrm{ES}}^{\mathrm{GS}}}\right)(1-\rho_{\mathrm{ES}}) - \frac{N_{\mathrm{ES}}}{\tau_{\mathrm{GS}}^{\mathrm{ES}}}(1-\rho_{\mathrm{GS}}) - \frac{N_{\mathrm{ES}}}{\tau_{\mathrm{RS}}^{\mathrm{ES}}} - \frac{N_{\mathrm{ES}}}{\tau_{\mathrm{ES}}^{\mathrm{spon}}} - \Gamma_p v_g g_{\mathrm{ES}} S_{\mathrm{ES}} + F_{\mathrm{ES}}, \tag{2}$$

$$\frac{\mathrm{d}N_{\mathrm{GS}}}{\mathrm{d}t} = \frac{N_{\mathrm{ES}}}{\tau_{\mathrm{GS}}^{\mathrm{ES}}}(1-\rho_{\mathrm{GS}}) - \frac{N_{\mathrm{GS}}}{\tau_{\mathrm{ES}}^{\mathrm{GS}}}(1-\rho_{\mathrm{ES}}) - \frac{N_{\mathrm{GS}}}{\tau_{\mathrm{GS}}^{\mathrm{spon}}} - \Gamma_p v_g g_{\mathrm{GS}} S_{\mathrm{GS}} + F_{\mathrm{GS}}, \tag{3}$$

$$\frac{\mathrm{d}S_{\mathrm{ES}}}{\mathrm{d}t} = \left(\Gamma_p v_g g_{\mathrm{ES}} - \frac{1}{\tau_p}\right) S_{\mathrm{ES}} + \beta_{\mathrm{sp}} \frac{N_{\mathrm{ES}}}{\tau_{\mathrm{ES}}^{\mathrm{spon}}} + F_{S_{\mathrm{ES}}} + 2\frac{k}{\tau_{\mathrm{in}}}\sqrt{S_{\mathrm{ES}}(t) S_{\mathrm{ES}}(t-\tau)}\cos(\Delta\phi_{\mathrm{ES}}), \tag{4}$$

$$\frac{\mathrm{d}S_{\mathrm{GS}}}{\mathrm{d}t} = \left(\Gamma_p v_g g_{\mathrm{GS}} - \frac{1}{\tau_p}\right) S_{\mathrm{GS}} + \beta_{\mathrm{sp}} \frac{N_{\mathrm{GS}}}{\tau_{\mathrm{GS}}^{\mathrm{spon}}} + F_{S_{\mathrm{GS}}} + 2\frac{k}{\tau_{\mathrm{in}}}\sqrt{S_{\mathrm{GS}}(t) S_{\mathrm{GS}}(t-\tau)}\cos(\Delta\phi_{\mathrm{GS}}), \tag{5}$$

$$\frac{\mathrm{d}\phi_{\mathrm{ES}}}{\mathrm{d}t} = \frac{1}{2}\Gamma_p v_g (g_{\mathrm{GS}}\kappa_{\mathrm{ES}}^{\mathrm{GS}} + g_{\mathrm{ES}}\alpha_{\mathrm{ES}} + g_{\mathrm{RS}}\kappa_{\mathrm{ES}}^{\mathrm{RS}}) + F_{\phi_{\mathrm{ES}}} - \frac{k}{\tau_{\mathrm{in}}}\sqrt{\frac{S_{\mathrm{ES}}(t-\tau)}{S_{\mathrm{ES}}(t)}}\sin(\Delta\phi_{\mathrm{ES}}), \tag{6}$$

$$\frac{\mathrm{d}\phi_{\mathrm{GS}}}{\mathrm{d}t} = \frac{1}{2}\Gamma_p v_g (g_{\mathrm{GS}}\alpha_{\mathrm{GS}} + g_{\mathrm{ES}}\kappa_{\mathrm{GS}}^{\mathrm{ES}} + g_{\mathrm{RS}}\kappa_{\mathrm{GS}}^{\mathrm{RS}}) + F_{\phi_{\mathrm{GS}}} - \frac{k}{\tau_{\mathrm{in}}}\sqrt{\frac{S_{\mathrm{GS}}(t-\tau)}{S_{\mathrm{GS}}(t)}}\sin(\Delta\phi_{\mathrm{GS}}), \tag{7}$$

where I is the injected bias current, β_{sp} is the spontaneous emission factor, q is the elementary charge, v_g is the group velocity, Γ_p is the optical confinement factor, τ_p is the photon lifetime, and $F_{\mathrm{RS,ES,GS}}$, $F_{S_{\mathrm{ES,GS}}}$, $F_{\phi_{\mathrm{ES,GS}}}$ are Langevin noise terms including carrier, photon, and phase noise sources, respectively. The optical feedback terms are included in the photon number and phase equations where τ_{in} and τ are the photon round trip time of the laser internal cavity and the optical feedback external cavity, respectively. k is the feedback coupling coefficient defined as $k = \frac{1-R}{\sqrt{R}}\sqrt{f_{\mathrm{ext}}}$, where f_{ext} is the feedback strength, and R is the facet reflectivity. The gains and the carrier occupation probabilities of each state are defined as

$$g_{\mathrm{RS}} = a_{\mathrm{RS}}\frac{D_{\mathrm{RS}}}{V_{\mathrm{RS}}}(2\rho_{\mathrm{RS}} - 1), \tag{8}$$

$$g_{ES} = \frac{a_{ES}}{1 + \xi_{ES} S_{ES}} \frac{N_B}{V_B} (2\rho_{ES} - 1), \tag{9}$$

$$g_{GS} = \frac{a_{GS}}{1 + \xi_{GS} S_{GS}} \frac{N_B}{V_B} (2\rho_{GS} - 1), \tag{10}$$

$$\rho_{RS} = \frac{N_{RS}}{D_{RS}}, \quad \rho_{ES} = \frac{N_{ES}}{4N_B}, \quad \rho_{GS} = \frac{N_{GS}}{2N_B}, \tag{11}$$

where $a_{RS,ES,GS}$ are the differential gains of each state, $\xi_{ES,GS}$ are the gain compression factors of ES and GS, D_{RS} is the total state number in RS, N_B is the total QD number, and V_{RS} and V_B are the volumes of the RS and active region, respectively. Feedback phase variation is expressed as

$$\Delta\phi_{ES} = \psi_{ES} + \phi_{ES}(t) - \phi_{ES}(t - \tau), \tag{12}$$

$$\Delta\phi_{GS} = \psi_{GS} + \phi_{GS}(t) - \phi_{GS}(t - \tau), \tag{13}$$

where $\psi_{ES,GS}$ are the initial phase shifts for ES and GS, respectively. They are given by the calculation result of free-running mode without feedback terms. Energy levels $E_{RS,ES,GS}$ play their roles through contribution coefficients as follows:

$$\kappa_{ES}^{RS,GS} = \frac{\omega_{ES}}{\omega_{RS,GS}} \frac{(\omega_{RS,GS} - \omega_{ES}) T_D}{1 + (\omega_{RS,GS} - \omega_{ES})^2 T_D^2}, \tag{14}$$

$$\kappa_{GS}^{RS,ES} = \frac{\omega_{GS}}{\omega_{RS,ES}} \frac{(\omega_{RS,ES} - \omega_{GS}) T_D}{1 + (\omega_{RS,ES} - \omega_{GS})^2 T_D^2}, \tag{15}$$

where angular frequency $\omega_{RS,ES,GS} = E_{RS,ES,GS}/\hbar$, and T_D is the dephasing time. It should be noted that E_{GS} is fixed to 0.82 eV, and $\Delta E_{ES}^{RS} = 2 \times \Delta E_{GS}^{ES}$, with ΔE_{GS}^{ES} being the ES-GS energy separation and ΔE_{ES}^{RS} the RS-ES energy separation. Thus, ES transition energy is given by $E_{ES} = E_{GS} + \Delta E_{GS}^{ES}$, and RS is expressed as $E_{RS} = E_{GS} + 3 \times \Delta E_{GS}^{ES}$. Other material and optical parameters of the QD laser used in the simulations are given in Table 1 if not otherwise specified [55,56].

Figure 6 demonstrates the GS and ES threshold current as well as ES-GS threshold ratio versus ES-GS energy separation ranging from 40 to 110 meV. It is noteworthy that the ES-GS energy separations of the QD laser up to 108 meV in measurement [57] and 126 meV in theory [58] have been demonstrated. The GS transition energy is mostly determined by the vertical confinement and thus the thickness of the QD, while energy separation is related to QD lateral confinement. For large ES-GS energy separation, the ES threshold increases while the GS threshold decreases followed by the increase of the ES-GS threshold ratio. This effect implies that high ES transition energy favors the maintenance of sole GS emission and delays the appearance of ES lasing; hence a high ES-GS energy separation is beneficial to increase the ES-GS threshold ratio in the fabrication of QD lasers. It is noted that the dependence of feedback resistance on the threshold ratio has been experimentally proved in epitaxial QD lasers on silicon [59]. Thus, the effect of ES-GS energy separation on reflection sensitivity is theoretically investigated as follows.

Table 1. Parameters Used in the Simulation

Symbol	Description	Value
E_{RS}	RS transition energy	0.97 eV
E_{ES}	ES transition energy	0.87 eV
E_{GS}	GS transition energy	0.82 eV
τ_{ES}^{RS}	RS to ES capture time	6.3 ps
τ_{GS}^{ES}	ES to GS relaxation time	2.9 ps
τ_{RS}^{ES}	ES to RS escape time	2.7 ns
τ_{ES}^{GS}	GS to ES escape time	10.4 ps
τ_{RS}^{spon}	RS spontaneous emission time	0.5 ns
τ_{ES}^{spon}	ES spontaneous emission time	0.5 ns
τ_{GS}^{spon}	GS spontaneous emission time	1.2 ns
ν_g	Group velocity	8.6×10^7 m/s
β_{sp}	Spontaneous emission factor	1.0×10^{-4}
Γ_p	Optical confinement factor	0.06
τ_p	Photon lifetime	4.1 ps
τ_{in}	Internal round trip time	11.7 ps
τ	External round trip time	2.0 ns
R	Facet reflectivity	0.32
a_{GS}	GS differential gain	5.0×10^{-15} cm^2
a_{ES}	ES differential gain	10×10^{-15} cm^2
a_{RS}	RS differential gain	2.5×10^{-15} cm^2
ξ_{ES}	ES gain compression factor	1.0×10^{-15} cm^3
ξ_{GS}	GS gain compression factor	1.0×10^{-15} cm^3
N_B	Total dot number	1.0×10^7
D_{RS}	Total RS state number	4.8×10^6
V_B	Active region volume	5.0×10^{-11} cm^3
V_{RS}	RS region volume	1.0×10^{-11} cm^3
T_D	Polarization dephasing time	0.1 ps

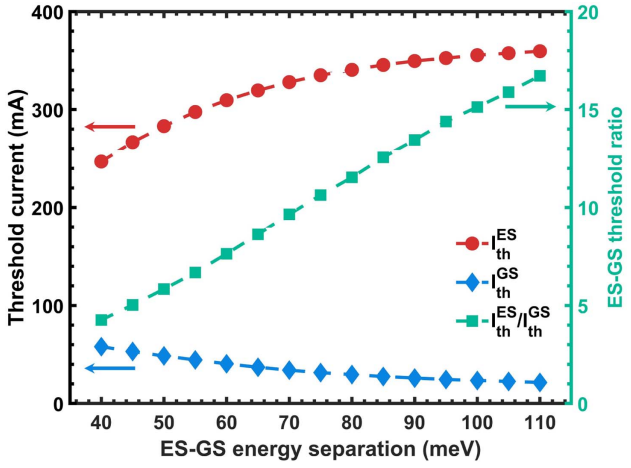

Fig. 6. GS threshold current, ES threshold current, and corresponding ES-GS threshold ratio with respect to ES-GS energy separation.

B. Optical Feedback Dynamics

The external cavity length is set to 30 cm in the simulation, in which case the QD laser is operated in the long-delay regime in line with the experiment [46,60,61]. Figure 7 shows

bifurcation diagrams with respect to the normalized bias current I/I_{th}^{ES} and ES-GS energy separation (ΔE_{GS}^{ES}). The corresponding time series and GS phase portraits are demonstrated in the second and third columns, respectively. Three values of ES-GS energy separation are applied to investigate the impact of energy separation on laser feedback sensitivity. In Fig. 7(a), the ES-GS energy separation is set to $\Delta E_{GS}^{ES} = 65$ meV, corresponding to $I_{th}^{GS} = 37.0$ mA, $I_{th}^{ES} = 319.5$ mA, and $I_{th}^{ES}/I_{th}^{GS} = 8.64$. The bifurcation diagram of GS lasing plots the case when the normalized bias current $I/I_{th}^{ES} = 1.0$, where the QD laser operates at the ES threshold. r_{crit} can be extracted from the first Hopf bifurcation, which is −26.3 dB. The time series and phase portrait of GS lasing are plotted with the high feedback strength of −12.0 dB, in which case the laser operates in a chaotic state with irregular time series peaks and overlapping phase portraits. Furthermore, the ES-GS energy separation is then set to $\Delta E_{GS}^{ES} = 80$ meV, corresponding to $I_{th}^{ES}/I_{th}^{GS} = 11.5$, and the normalized bias current is set to $I/I_{th}^{ES} = 1.31$ in Fig. 7(b). The QD laser operates in the dual-state lasing regime where both GS and ES show the same r_{crit} of −14.3 dB. The time series with a feedback strength of −11.0 dB illustrates that period-one periodic oscillation is taking place for both GS and ES; the corresponding GS portrait gives one closed circle approximating a line. Figure 7(c1) reveals the bifurcation diagram for large ΔE_{GS}^{ES} of 110 meV at $I/I_{th}^{ES} = 0.87$, indicating that the laser operates at sole GS. The corresponding I_{th}^{ES}/I_{th}^{GS} is 16.7, and r_{crit} is −20.3 dB. Figures 7(c2) and 7(c3) show the time series and phase portrait for f_{ext} of −13.0 dB, where the period-two periodic oscillation is found in the time domain with two closed circles in the phase portrait.

Figure 8 compares the critical feedback levels extracted at different bias currents between measurement and simulation. For the measurement, the minimum r_{crit} is found at the ES threshold current, while r_{crit} is enhanced regardless of whether the bias current is increased or decreased, which means that the QD laser has higher resistance to optical feedback at bias currents away from the ES threshold. The influence of ES-GS energy separation on the resistance to optical feedback is also demonstrated in Fig. 8. When the ES-GS energy separation is set to 65 meV, which is the same as the result of the QD material grown by the same technology [62], the simulation

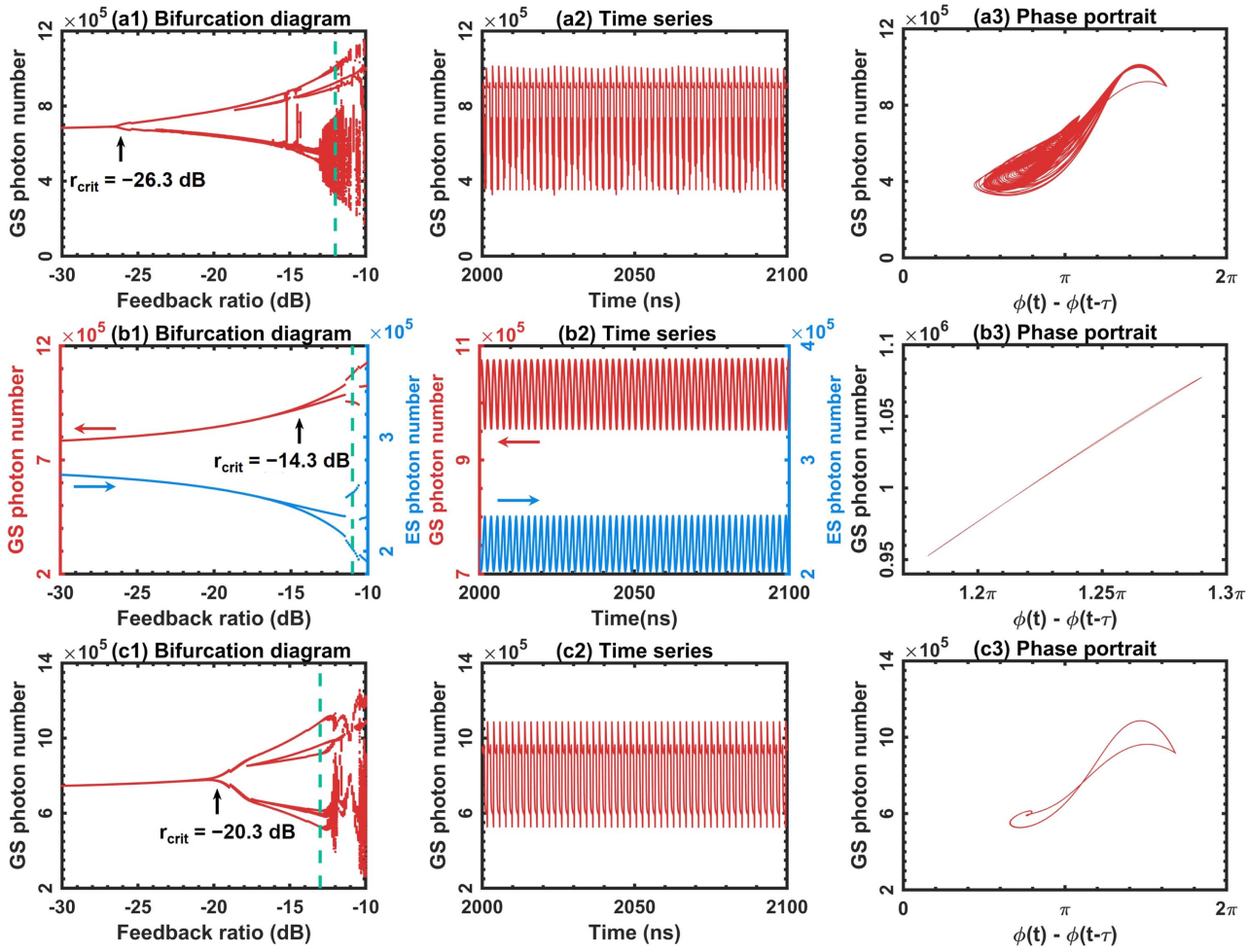

Fig. 7. Samples of the bifurcation diagrams (column 1), time series (column 2), and GS phase portraits (column 3). (a) $\Delta E_{GS}^{ES} = 65$ meV, $I/I_{th}^{ES} = 1.0$, and $f_{ext} = -12.0$ dB; (b) $\Delta E_{GS}^{ES} = 80$ meV, $I/I_{th}^{ES} = 1.31$, and $f_{ext} = -11.0$ dB; (c) $\Delta E_{GS}^{ES} = 110$ meV, $I/I_{th}^{ES} = 0.87$, and $f_{ext} = -13.0$ dB. Green vertical dashed lines in the first column mark the f_{ext} taken in the second and third columns; r_{crit} extracted from the bifurcation diagrams are marked in the first column.

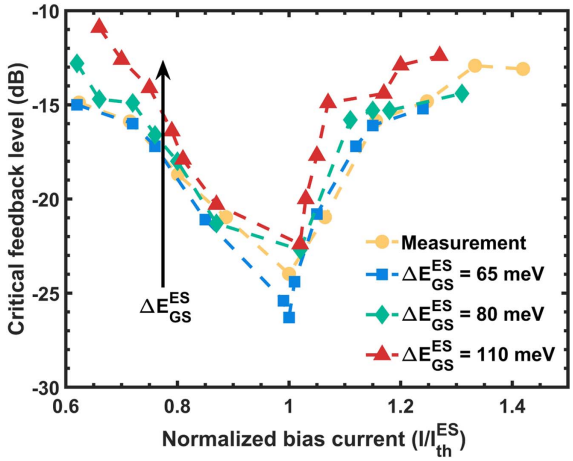

Fig. 8. Critical feedback levels as a function of normalized bias currents ($I/I_{\text{th}}^{\text{ES}}$). Triangles, diamonds, and squares are numerically calculated for different ES-GS energy separations, while the dots are extracted from measurement results.

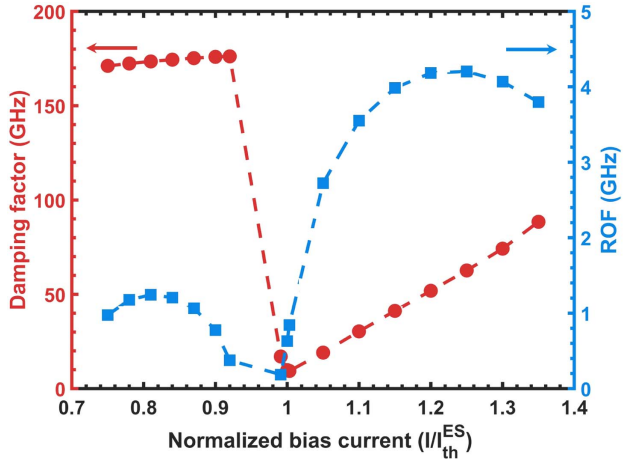

Fig. 10. Damping factor and relaxation oscillation frequency versus normalized bias currents ($I/I_{\text{th}}^{\text{ES}}$).

results are quantitatively in agreement with the measurement. Therefore, the validity of the dual-state QD lasers model under optical feedback is verified. The black arrow confirms that a large $\Delta E_{\text{GS}}^{\text{ES}}$ strengthens the laser stability against optical feedback. For instance, at 1.05 $\times I_{\text{th}}^{\text{ES}}$ near the ES threshold, r_{crit} increases from −20.8 dB for $\Delta E_{\text{GS}}^{\text{ES}} = 65$ meV to −17.7 dB for $\Delta E_{\text{GS}}^{\text{ES}} = 110$ meV. In dual-state lasing operation, r_{crit} reaches −12.4 dB for the laser with $\Delta E_{\text{GS}}^{\text{ES}}$ of 110 meV at 1.27 $\times I_{\text{th}}^{\text{ES}}$. Since $I_{\text{th}}^{\text{ES}}/I_{\text{th}}^{\text{GS}}$ is positively correlated with $\Delta E_{\text{GS}}^{\text{ES}}$, Fig. 8 also indicates that large ES-GS energy separation, which can be obtained by optimizing the size, composition, and strained buffer layer of the QDs [57,58,63,64], contributes to maintaining the sole GS emission at high bias current and attenuates the reflection sensitivity in the case of dual-state lasing.

C. Linewidth Enhancement Factor and Damping Factor

The dynamic properties of QD lasers including α_H-factor, damping factor, and ROF are investigated to explain the high feedback sensitivity at the ES threshold. Figure 9 displays that

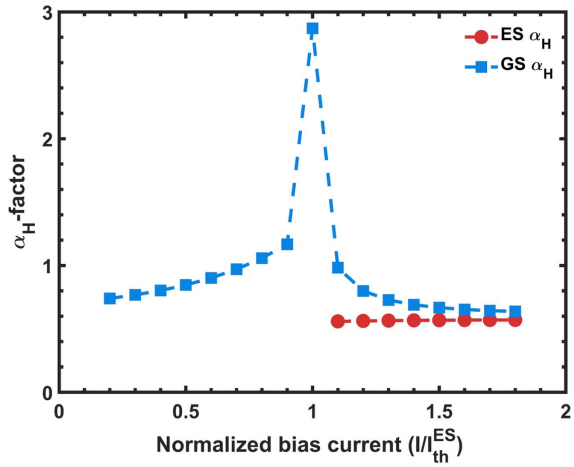

Fig. 9. Linewidth enhancement factor as a function of normalized bias currents ($I/I_{\text{th}}^{\text{ES}}$) for GS and ES, respectively.

the dependence of normalized bias current on the α_H-factor originates from the GS and ES. The α_H-factors are obtained from the phase noise spectrum, while $\Delta E_{\text{GS}}^{\text{ES}}$ is set to 50 meV [65]. The α_H of GS grows from 0.7 at 0.2 × $I_{\text{th}}^{\text{ES}}$ to 1.2 at 0.9 × $I_{\text{th}}^{\text{ES}}$ and then exhibits a peak of 2.9 at the ES threshold current, which is attributed to the enhanced carrier variation in the RS and ES [26,66]. As the bias current continues to increase above the ES threshold, the carriers in ES are clamped, which suppresses the carrier variation in ES [67]. Therefore, GS α_H decreases from 1.0 at 1.1 × $I_{\text{th}}^{\text{ES}}$ to 0.6 at 1.8 × $I_{\text{th}}^{\text{ES}}$, while ES α_H remains constant at about 0.57. This difference depicts that feedback sensitivity is mainly driven by the α_H from the GS.

The damping factor and ROF extracted from the modulation transfer function of the laser system, are shown in Fig. 10 as a function of the normalized bias current. With the increase of bias current, the laser is overdamped with a high damping factor slightly increasing from 171 to 176 GHz, and the ROF increases to a maximum of 1.24 GHz. Nevertheless, a sharp decline in the damping factor is observed, reaching its minimum value of 9.4 GHz, and the ROF is also a minimum of 0.2 GHz. This remarkable reduction can be attributed to the predominant influence of ES spontaneous emission. As the ES lasing threshold is surpassed, the stimulated emission from ES becomes dominant, subsequently amplifying both the damping factor and the ROF. r_{crit} can be calculated by [4,68,69]

$$r_{\text{crit}} = \frac{\gamma^2(1+\alpha_H^2)}{\alpha_H^4}\frac{\tau_{\text{in}}^2 R}{4(1-R)^2}, \tag{16}$$

where γ is the damping factor. Therefore, it is verified that the local minimum value of r_{crit} at the ES threshold shown in Fig. 8 is driven by high α_H-factor, low damping factor, and low ROF, which result in the reflection sensitivity of the QD laser.

4. CONCLUSION

We investigated the reflection sensitivity of dual-state QD lasers from both measurements and simulations. The experimental results demonstrate that the r_{crit} of dual-state QD lasers

strongly depends on the occurrence of the ES, and the feedback tolerance is significantly degraded at the ES lasing threshold. The numerical model of dual-state QD lasers considering external optical feedback is established to investigate this phenomenon. r_{crit} extracted from the bifurcation diagram is in good agreement with the measurement, which confirms the validity of the model. Furthermore, the high ES-GS energy-level separation associated with the high ES-GS threshold ratio contributes to strengthening the feedback resistance. At the ES threshold, the burst α_H-factor and the collapse damping factor make the QD laser more sensitive to external optical feedback. These findings bring new insights for understanding the physical mechanisms in QD lasers and highlight the importance of energy-level engineering in fabricating reflection-insensitive dual-state QD lasers for isolator-free PICs. Future work will focus on the optical noise properties of dual-state QD lasers under optical feedback.

Funding. National Key Research and Development Program of China (2022YFB2803600); National Natural Science Foundation of China (62204072, U22A2093); Basic and Applied Basic Research Foundation of Guangdong Province (2021A1515110076, 2023A1515012304); Shenzhen Science and Technology Innovation Program (GXWD20220811163623002, RCBS20210609103824050).

Acknowledgment. We acknowledge Professor Dieter Bimberg from Technische Universität Berlin, Germany, and Changchun Institute of Optics, Fine Mechanics and Physics, Chinese Academy of Sciences, China, for providing the high-quality QD laser sample.

Disclosures. The authors declare no conflicts of interest.

Data Availability. Data underlying the results presented in this paper are not publicly available at this time but may be obtained from the authors upon reasonable request.

REFERENCES

1. J. E. Bowers, L. Chang, M. Li, Q. Lin, W. Xie, X. Wang, H. Shu, and K. Vahala, "Silicon photonic integrated circuits for LiDAR," in *IEEE Photonics Conference (IPC)* (IEEE, 2022), pp. 1–3.
2. B. J. Shastri, A. N. Tait, T. Ferreira de Lima, W. H. Pernice, H. Bhaskaran, C. D. Wright, and P. R. Prucnal, "Photonics for artificial intelligence and neuromorphic computing," Nat. Photonics **15**, 102–114 (2021).
3. J. Wang, F. Sciarrino, A. Laing, and M. G. Thompson, "Integrated photonic quantum technologies," Nat. Photonics **14**, 273–284 (2020).
4. Y.-G. Zhou, X.-Y. Zhao, C.-F. Cao, Q. Gong, and C. Wang, "High optical feedback tolerance of InAs/GaAs quantum dot lasers on germanium," Opt. Express **26**, 28131–28139 (2018).
5. Z. Zhang, D. Jung, J. C. Norman, W. W. Chow, and J. E. Bowers, "Linewidth enhancement factor in InAs/GaAs quantum dot lasers and its implication in isolator-free and narrow linewidth applications," IEEE J. Sel. Top. Quantum Electron. **25**, 1900509 (2019).
6. F. Grillot, J. C. Norman, J. Duan, Z. Zhang, B. Dong, H. Huang, W. W. Chow, and J. E. Bowers, "Physics and applications of quantum dot lasers for silicon photonics," Nanophotonics **9**, 1271–1286 (2020).
7. Y. Arakawa, T. Nakamura, and J. Kwoen, "Chapter Three—Quantum dot lasers for silicon photonics," in *Future Directions in Silicon Photonics*, Semiconductors and Semimetals, S. Lourdudoss, J. E. Bowers, and C. Jagadish, eds. (Elsevier, 2019), Vol. **101**, pp. 91–138.
8. F. Grillot, J. Duan, B. Dong, and H. Huang, "Uncovering recent progress in nanostructured light-emitters for information and communication technologies," Light Sci. Appl. **10**, 156 (2021).
9. J. C. Norman, D. Jung, Y. Wan, and J. E. Bowers, "Perspective: the future of quantum dot photonic integrated circuits," APL Photon. **3**, 030901 (2018).
10. C. Shang, Y. Wan, J. Selvidge, E. Hughes, R. Herrick, K. Mukherjee, J. Duan, F. Grillot, W. W. Chow, and J. E. Bowers, "Perspectives on advances in quantum dot lasers and integration with Si photonic integrated circuits," ACS Photon. **8**, 2555–2566 (2021).
11. Y. Du, B. Xu, G. Wang, Y. Miao, B. Li, Z. Kong, Y. Dong, W. Wang, and H. H. Radamson, "Review of highly mismatched III-V heteroepitaxy growth on (001) silicon," Nanomaterials **12**, 741 (2022).
12. A. Y. Liu, C. Zhang, J. Norman, A. Snyder, D. Lubyshev, J. M. Fastenau, A. W. Liu, A. C. Gossard, and J. E. Bowers, "High performance continuous wave 1.3 μm quantum dot lasers on silicon," Appl. Phys. Lett. **104**, 041104 (2014).
13. J. Duan, H. Huang, D. Jung, Z. Zhang, J. Norman, J. Bowers, and F. Grillot, "Semiconductor quantum dot lasers epitaxially grown on silicon with low linewidth enhancement factor," Appl. Phys. Lett. **112**, 251111 (2018).
14. C. R. Fitch, I. P. Marko, A. Baltušis, D. Jung, J. C. Norman, J. E. Bowers, and S. J. Sweeney, "Carrier recombination properties of low-threshold 1.3 μm quantum dot lasers on silicon," IEEE J. Sel. Top. Quantum Electronics **28**, 1900210 (2021).
15. C. Jiang, H. Liu, J. Wang, X. Ren, Q. Wang, Z. Liu, B. Ma, K. Liu, R. Ren, Y. Zhang, S. Cai, and Y. Huang, "Demonstration of room-temperature continuous-wave operation of InGaAs/AlGaAs quantum well lasers directly grown on on-axis silicon (001)," Appl. Phys. Lett. **121**, 061102 (2022).
16. Z.-R. Lv, S. Wang, H. Wang, H.-M. Wang, H.-Y. Chai, X.-G. Yang, L. Meng, C. Ji, and T. Yang, "Significantly improved performances of 1.3 μm InAs/GaAs QD laser by spatially separated dual-doping," Appl. Phys. Lett. **121**, 021105 (2022).
17. D. Arsenijević and D. Bimberg, "Quantum-dot lasers for 35 Gbit/s pulse-amplitude modulation and 160 Gbit/s differential quadrature phase-shift keying," Proc. SPIE **9892**, 98920S (2016).
18. S. Banyoudeh, A. Abdollahinia, O. Eyal, F. Schnabel, V. Sichkovskyi, G. Eisenstein, and J. P. Reithmaier, "Temperature-insensitive high-speed directly modulated 1.55-μm quantum dot lasers," IEEE Photon. Technol. Lett. **28**, 2451–2454 (2016).
19. H. Huang, J. Duan, B. Dong, J. Norman, D. Jung, J. Bowers, and F. Grillot, "Epitaxial quantum dot lasers on silicon with high thermal stability and strong resistance to optical feedback," APL Photon. **5**, 016103 (2020).
20. M. Buffolo, L. Rovere, C. De Santi, D. Jung, J. Norman, J. E. Bowers, R. W. Herrick, G. Meneghesso, E. Zanoni, and M. Meneghini, "Degradation of 1.3 μm InAs quantum-dot laser diodes: Impact of dislocation density and number of quantum dot layers," IEEE J. Quantum Electron. **57**, 2000108 (2020).
21. J. Duan, Y. Zhou, B. Dong, H. Huang, J. C. Norman, D. Jung, Z. Zhang, C. Wang, J. E. Bowers, and F. Grillot, "Effect of p-doping on the intensity noise of epitaxial quantum dot lasers on silicon," Opt. Lett. **45**, 4887–4890 (2020).
22. Z. Yang, Z. Ding, L. Liu, H. Zhong, S. Cao, X. Zhang, S. Lin, X. Huang, H. Deng, Y. Yu, and S. Yu, "High-performance distributed feedback quantum dot lasers with laterally coupled dielectric gratings," Photon. Res. **10**, 1271–1279 (2022).
23. A. Markus, J. X. Chen, O. Gauthier-Lafaye, J.-G. Provost, C. Paranthoën, and A. Fiore, "Impact of intraband relaxation on the performance of a quantum-dot laser," IEEE J. Sel. Top. Quantum Electron. **9**, 1308–1314 (2003).
24. E. A. Viktorov, P. Mandel, Y. Tanguy, J. Houlihan, and G. Huyet, "Electron-hole asymmetry and two-state lasing in quantum dot lasers," Appl. Phys. Lett. **87**, 053113 (2005).
25. A. Roehm, B. Lingnau, and K. Luedge, "Understanding ground-state quenching in quantum-dot lasers," IEEE J. Quantum Electron. **51**, 2000211 (2014).
26. C. Wang, B. Lingnau, K. Lüdge, J. Even, and F. Grillot, "Enhanced dynamic performance of quantum dot semiconductor lasers operating on the excited state," IEEE J. Quantum Electron. **50**, 723–731 (2014).

27. D. Arsenijević, A. Schliwa, H. Schmeckebier, M. Stubenrauch, M. Spiegelberg, D. Bimberg, V. Mikhelashvili, and G. Eisenstein, "Comparison of dynamic properties of ground- and excited-state emission in p-doped InAs/GaAs quantum-dot lasers," Appl. Phys. Lett. **104**, 181101 (2014).
28. B. Stevens, D. Childs, H. Shahid, and R. Hogg, "Direct modulation of excited state quantum dot lasers," Appl. Phys. Lett. **95**, 061101 (2009).
29. H. Huang, D. Arsenijević, K. Schires, T. Sadeev, D. Bimberg, and F. Grillot, "Multimode optical feedback dynamics of InAs/GaAs quantum-dot lasers emitting on different lasing states," AIP Adv. **6**, 125114 (2016).
30. H. Huang, L.-C. Lin, C.-Y. Chen, D. Arsenijević, D. Bimberg, F.-Y. Lin, and F. Grillot, "Multimode optical feedback dynamics in InAs/GaAs quantum dot lasers emitting exclusively on ground or excited states: transition from short- to long-delay regimes," Opt. Express **26**, 1743–1751 (2018).
31. L.-C. Lin, C.-Y. Chen, H. Huang, D. Arsenijević, D. Bimberg, F. Grillot, and F.-Y. Lin, "Comparison of optical feedback dynamics of InAs/GaAs quantum-dot lasers emitting solely on ground or excited states," Opt. Lett. **43**, 210–213 (2018).
32. C.-G. Ma, J.-L. Xiao, Z.-X. Xiao, Y.-D. Yang, and Y.-Z. Huang, "Chaotic microlasers caused by internal mode interaction for random number generation," Light Sci. Appl. **11**, 187 (2022).
33. R. Pawlus, L. Columbo, P. Bardella, S. Breuer, and M. Gioannini, "Intensity noise behavior of an InAs/InGaAs quantum dot laser emitting on ground states and excited states," Opt. Lett. **43**, 867–870 (2018).
34. A. Röhm, B. Lingnau, and K. Lüdge, "Ground-state modulation-enhancement by two-state lasing in quantum-dot laser devices," Appl. Phys. Lett. **106**, 191102 (2015).
35. Z.-R. Lv, H.-M. Ji, S. Luo, F. Gao, F. Xu, D.-H. Xiao, and T. Yang, "Dynamic characteristics of two-state lasing quantum dot lasers under large signal modulation," AIP Adv. **5**, 107115 (2015).
36. Y. Xiong and X. Zhang, "Two-state lasing at room temperature in InAs/InP quantum dots," J. Appl. Phys. **126**, 133102 (2019).
37. B. Kelleher, M. Dillane, and E. A. Viktorov, "Optical information processing using dual state quantum dot lasers: complexity through simplicity," Light Sci. Appl. **10**, 238 (2021).
38. B. Tykalewicz, D. Goulding, S. P. Hegarty, G. Huyet, D. Byrne, R. Phelan, and B. Kelleher, "All-optical switching with a dual-state, single-section quantum dot laser via optical injection," Opt. Lett. **39**, 4607–4610 (2014).
39. E. Viktorov, I. Dubinkin, N. Fedorov, T. Erneux, B. Tykalewicz, S. Hegarty, G. Huyet, D. Goulding, and B. Kelleher, "Injection-induced, tunable all-optical gating in a two-state quantum dot laser," Opt. Lett. **41**, 3555–3558 (2016).
40. M. T. Hill, H. J. Dorren, T. De Vries, X. J. Leijtens, J. H. Den Besten, B. Smalbrugge, Y.-S. Oei, H. Binsma, G.-D. Khoe, and M. K. Smit, "A fast low-power optical memory based on coupled micro-ring lasers," Nature **432**, 206–209 (2004).
41. C. Zhang, D. Liang, G. Kurczveil, A. Descos, and R. G. Beausoleil, "Hybrid quantum-dot microring laser on silicon," Optica **6**, 1145–1151 (2019).
42. R. S. Gajjela, A. L. Hendriks, J. O. Douglas, E. M. Sala, P. Steindl, P. Klenovský, P. A. Bagot, M. P. Moody, D. Bimberg, and P. M. Koenraad, "Structural and compositional analysis of (InGa)(AsSb)/GaAs/GaP Stranski–Krastanov quantum dots," Light Sci. Appl. **10**, 125 (2021).
43. M. Raburn, M. Takenaka, K. Takeda, X. Song, J. S. Barton, and Y. Nakano, "Integrable multimode interference distributed Bragg reflector laser all-optical flip-flops," IEEE Photon. Technol. Lett. **18**, 1421–1423 (2006).
44. B. Garbin, D. Goulding, S. Hegarty, G. Huyet, B. Kelleher, and S. Barland, "Incoherent optical triggering of excitable pulses in an injection-locked semiconductor laser," Opt. Lett. **39**, 1254–1257 (2014).
45. M. Dillane, B. Lingnau, E. Viktorov, I. Dubinkin, N. Fedorov, and B. Kelleher, "Asymmetric excitable phase triggering in an optically injected semiconductor laser," Opt. Lett. **46**, 440–443 (2021).
46. B. Dong, J. Duan, H. Huang, J. C. Norman, K. Nishi, K. Takemasa, M. Sugawara, J. E. Bowers, and F. Grillot, "Dynamic performance and reflection sensitivity of quantum dot distributed feedback lasers with large optical mismatch," Photon. Res. **9**, 1550–1558 (2021).
47. J. Duan, H. Huang, B. Dong, D. Jung, J. C. Norman, J. E. Bowers, and F. Grillot, "1.3-μm reflection insensitive InAs/GaAs quantum dot lasers directly grown on silicon," IEEE Photon. Technol. Lett. **31**, 345–348 (2019).
48. S. Ding, B. Dong, H. Huang, J. E. Bowers, and F. Grillot, "Reflection sensitivity of InAs/GaAs epitaxial quantum dot lasers under direct modulation," Electron. Lett. **58**, 363–365 (2022).
49. Y. Arakawa, T. Nakamura, and K. Kurata, "Highlights of 10-years of research in a Japanese Si photonics project," in *Optical Fiber Communication Conference* (Optica, 2022), paper Th3C-6.
50. E. A. Viktorov, P. Mandel, I. O'Driscoll, O. Carroll, G. Huyet, J. Houlihan, and Y. Tanguy, "Low-frequency fluctuations in two-state quantum dot lasers," Opt. Lett. **31**, 2302–2304 (2006).
51. M. Virte, K. Panajotov, and M. Sciamanna, "Mode competition induced by optical feedback in two-color quantum dot lasers," IEEE J. Quantum Electron. **49**, 578–585 (2013).
52. M. Virte, S. Breuer, M. Sciamanna, and K. Panajotov, "Switching between ground and excited states by optical feedback in a quantum dot laser diode," Appl. Phys. Lett. **105**, 121109 (2014).
53. A. Kovsh, N. Maleev, A. Zhukov, S. Mikhrin, A. Vasil'ev, E. Semenova, Y. M. Shernyakov, M. Maximov, D. Livshits, V. Ustinov, N. N. Ledentsov, D. Bimberg, and Z. L. Alferov, "InAs/InGaAs/GaAs quantum dot lasers of 1.3 μm range with enhanced optical gain," J. Cryst. Growth **251**, 729–736 (2003).
54. B. Dong, J.-D. Chen, F.-Y. Lin, J. C. Norman, J. E. Bowers, and F. Grillot, "Dynamic and nonlinear properties of epitaxial quantum-dot lasers on silicon operating under long-and short-cavity feedback conditions for photonic integrated circuits," Phys. Rev. A **103**, 033509 (2021).
55. C. Wang, M. Osiński, J. Even, and F. Grillot, "Phase-amplitude coupling characteristics in directly modulated quantum dot lasers," Appl. Phys. Lett. **105**, 221114 (2014).
56. Y. Zhou, J. Duan, F. Grillot, and C. Wang, "Optical noise of dual-state lasing quantum dot lasers," IEEE J. Quantum Electron. **56**, 2001207 (2020).
57. Y. Wei, S. Wang, F. Ferdos, J. Vukusic, A. Larsson, Q. Zhao, and M. Sadeghi, "Large ground-to-first-excited-state transition energy separation for InAs quantum dots emitting at 1.3 μm," Appl. Phys. Lett. **81**, 1621–1623 (2002).
58. Y. Gu, T. Yang, H. Ji, P. Xu, and Z. Wang, "Redshift and discrete energy level separation of self-assembled quantum dots induced by strain-reducing layer," J. Appl. Phys. **109**, 064320 (2011).
59. H. Huang, J. Duan, D. Jung, A. Y. Liu, Z. Zhang, J. Norman, J. E. Bowers, and F. Grillot, "Analysis of the optical feedback dynamics in InAs/GaAs quantum dot lasers directly grown on silicon," J. Opt. Soc. Am. B **35**, 2780–2787 (2018).
60. T. Heil, I. Fischer, W. Elsäßer, and A. Gavrielides, "Dynamics of semiconductor lasers subject to delayed optical feedback: the short cavity regime," Phys. Rev. Lett. **87**, 243901 (2001).
61. S. Zhao and F. Grillot, "Effect of Shockley-Read-Hall recombination on the static and dynamical characteristics of epitaxial quantum-dot lasers on silicon," Phys. Rev. A **103**, 063521 (2021).
62. P. Borri, W. Langbein, S. Schneider, U. Woggon, R. L. Sellin, D. Ouyang, and D. Bimberg, "Ultralong dephasing time in InGaAs quantum dots," Phys. Rev. Lett. **87**, 157401 (2001).
63. O. B. Shchekin, G. Park, D. L. Huffaker, and D. G. Deppe, "Discrete energy level separation and the threshold temperature dependence of quantum dot lasers," Appl. Phys. Lett. **77**, 466–468 (2000).
64. H. Liu and M. Hopkinson, "Tuning the structural and optical properties of 1.3-μm InAs/GaAs quantum dots by a combined InAlAs and GaAs strained buffer layer," Appl. Phys. Lett. **82**, 3644–3646 (2003).
65. J. Duan, X.-G. Wang, Y.-G. Zhou, C. Wang, and F. Grillot, "Carrier-noise-enhanced relative intensity noise of quantum dot lasers," IEEE J. Quantum Electron. **54**, 2001407 (2018).

66. C. Wang, J.-P. Zhuang, F. Grillot, and S.-C. Chan, "Contribution of off-resonant states to the phase noise of quantum dot lasers," Opt. Express **24**, 29872–29881 (2016).
67. F. Grillot, , B. Dagens, J.-G. Provost, H. Su, and L. F. Lester, "Gain compression and above-threshold linewidth enhancement factor in 1.3-μm InAs-GaAs quantum-dot lasers," IEEE J. Quantum Electron. **44**, 946–951 (2008).
68. J. Helms and K. Petermann, "A simple analytic expression for the stable operation range of laser diodes with optical feedback," IEEE J. Quantum Electron. **26**, 833–836 (1990).
69. J. O. Binder and G. D. Cormack, "Mode selection and stability of a semiconductor laser with weak optical feedback," IEEE J. Quantum Electron. **25**, 2255–2259 (1989).